Article

Acrylate Formation via Metal-Assisted C–C Coupling between CO and CH: Reaction Mechanism as Revealed from Density Functional Calculations

Gbor Schubert, and Imre Ppai

J. Am. Chem. Soc., **2003**, 125 (48), 14847-14858• DOI: 10.1021/ja035791u • Publication Date (Web): 11 November 2003

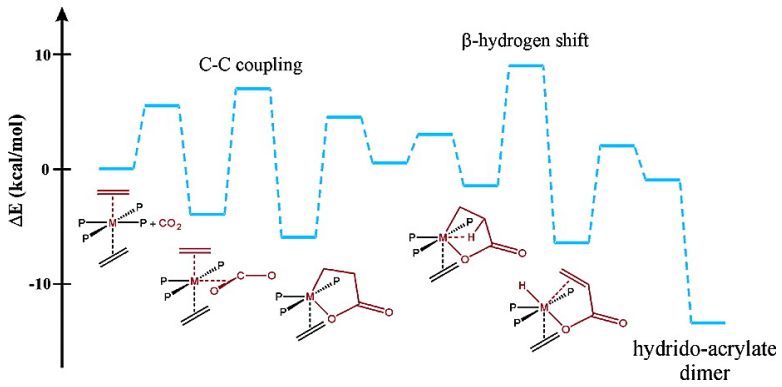

More About This Article

Additional resources and features associated with this article are available within the HTML version:

- Supporting Information
- Links to the 5 articles that cite this article, as of the time of this article download
- Access to high resolution figures
- Links to articles and content related to this article
- Copyright permission to reproduce figures and/or text from this article

View the Full Text HTML

J|A|C|S
ARTICLES
Published on Web 11/11/2003

Acrylate Formation via Metal-Assisted C−C Coupling between CO_2 and C_2H_4: Reaction Mechanism as Revealed from Density Functional Calculations

Gábor Schubert and Imre Pápai*

Contribution from the Institute of Chemistry, Theoretical Chemistry Department, Chemical Research Center of HAS, Pusztaszeri út 59-67, H-1025 Budapest, Hungary

Received April 25, 2003; E-mail: papai@chemres.hu

Abstract: The reaction path for the formation of a binuclear hydrido-acrylate complex in a $CO_2-C_2H_4$ coupling process is explored in detail by locating the key intermediates and transition states on model potential energy surfaces derived from density functional calculations on realistic models. The formation of the new C−C bond is shown to take place via oxidative coupling of coordinated CO_2 and C_2H_4 ligands resulting in a metalla-lactone intermediate, which can rearrange to an agostic species allowing for a β-hydrogen shift process. The overall reaction is predicted to be clearly exothermic with all intermediates lying below the reactants in energy, and the highest barrier steps correspond to C−C coupling and β-hydrogen transfer. The phosphine ligands are found to play an important role in various phases of the reaction as their dissociation controls the coordination of CO_2, the formation of the agostic intermediate, and the dimerization process; furthermore, their presence facilitates the oxidative coupling by supplying electrons to the metal center. Our results provide a theoretical support for the reaction mechanism proposed from experimental observations. The effect of the solvent medium on the relative energy of reaction intermediates and transition states is examined and found important in order to predict reliable energetics.

1. Introduction

The utilization of carbon dioxide as a feedstock in synthetic chemistry has been of continuous interest in the past decades, and its importance is ever-increasing. Despite the enormous efforts put forth in developing preparative methods in this field,[1−8] there are only a few examples of large-scale CO_2 utilization in synthetic chemistry.[9] To establish economically operating technologies, the activation of CO_2 ought to be combined with higher energy substances. This approach has led to the development of promising catalytic methods, for instance, in the synthesis of polycarbonates from the reactions of CO_2 with epoxides,[10,11] but other coupling processes hold great promise as well. Among those are the homogeneous catalytic reactions with unsaturated hydrocarbons, particularly with olefins and dienes, which have been extensively investigated with the above objectives.[2,3,5,7,8]

The first results on successful catalytic C−C coupling reactions were reported in the late 1970s by Inoue et al.,[12,13] who synthesized γ-lactones in low yield by the reaction of butadiene with CO_2. These results were followed by extensive studies on further catalytic CO_2-coupling reactions including coupling with other dienes (1,3-dienes, allene, isoprene), as well as with different monoenes, and a variety of ester and lactone products were synthesized.[2,3,5] To identify possible intermediates in these catalytic processes, stoichiometric CO_2-olefin coupling reactions were also investigated.[2,3,5] Most of the olefins were generally found to undergo oxidative coupling reactions with CO_2 in the presence of transition metal centers such as Ni, Fe, and Ti[14−21] giving rise to five-membered metallacycles (Scheme

(1) Palmer, D. A.; van Eldik, R. *Chem. Rev.* **1983**, *83*, 651.
(2) Behr, A. *Angew. Chem., Int. Ed. Engl.* **1988**, *27*, 661.
(3) Braunstein, P.; Matt, D.; Nobel, D. *Chem. Rev.* **1988**, *88*, 747.
(4) Aresta, M., Schloss, J. V., Eds. *Enzymatic and Model Carboxylation and Reduction Reactions for Carbon Dioxide Utilization*; NATO ASI Ser. C, 314; Kluwer: Dordrecht, the Netherlands, 1990.
(5) Leitner, W. *Coord. Chem. Rev.* **1996**, *153*, 257.
(6) Gibson, D. H. *Chem. Rev.* **1996**, *96*, 2063.
(7) Yin, X.; Moss, J. R. *Coord. Chem. Rev.* **1999**, *181*, 27.
(8) Song, C., Gaffney, A. M., Fujimoto, K., Eds. *CO_2 Conversion and Utilization*; ACS Symposium Series 809; American Chemical Society: Washington, DC, 2002.
(9) Arakawa, H.; Aresta, M.; Armor, J. N.; Barteau, M. A.; Beckman, E. J.; Bell, A. T.; Bercaw, J. E.; Creutz, C.; Dinjus, E.; Dixon, D. A.; Domen, K.; Dubois, D. L.; Eckert, J.; Fujita, E.; Gibson, D. H.; Goddard, W. A.; Goodman, D. W.; Keller, J.; Kubas, G. J.; Kung, H. H.; Lyons, J. E.; Manzer, L. E.; Marks, T. J.; Morokuma, K.; Nicholas, K. M.; Periana, R.; Que, L.; Rostrup-Nielson, J.; Sachtler, W. M. H.; Schmidt, L. D.; Sen, A.; Somorjai, G. A.; Stair, P. C.; Stults, B. R.; Tumas, W. *Chem. Rev.* **2001**, *101*, 953.
(10) For reviews on CO_2/epoxide copolymerization, see: (a) Darensbourg, D. J.; Holtcamp, M. W. *Coord. Chem. Rev.* **1996**, *153*, 155. (b) Super, M.; Beckman, E. *Trends Polym. Sci.* **1997**, *5*, 236. (c) Kuran, W. *Prog. Polym. Sci.* **1998**, *23*, 919.
(11) For the most recent achievements, see: (a) Darensbourg, D. J.; Yarbrough, J. C. *J. Am. Chem. Soc.* **2002**, *124*, 6335. (b) Allen, S. D.; Moore, D. R.; Lobkovsky, E. B.; Coates, G. W. *J. Am. Chem. Soc.* **2002**, *124*, 14284. (c) Paddock, R. L.; Nguyen, S. T. *J. Am. Chem. Soc.* **2001**, *123*, 11498. (d) Cheng, M.; Moore, D. R.; Reczek, J. J.; Chamberlain, B. M.; Lobkovsky, E. B.; Coates, G. W. *J. Am. Chem. Soc.* **2001**, *123*, 8738.
(12) Sasaki, Y.; Inoue, Y.; Hashimoto, H. *J. Chem. Soc., Chem. Commun.* **1976**, 605.
(13) Inoue, Y.; Sasaki, Y.; Hashimoto, H. *Bull. Chem. Soc. Jpn.* **1978**, *51*, 2375.
(14) Dinjus, E.; Walther, D.; Schütz, H. *Z. Chem.* **1983**, *23*, 408.
(15) Hoberg, H.; Schäfer, D.; Burkhart, G.; Krüger, C.; Romão, M. J. *J. Organomet. Chem.* **1984**, *266*, 203.
(16) Walther, D.; Dinjus, E.; Sieler, J.; Andersen, L.; Lindquist, O. *J. Organomet. Chem.* **1984**, *276*, 99.
(17) Hoberg, H.; Schaefer, D.; Oster, B. W. *J. Organomet. Chem.* **1984**, *266*, 313.
(18) Cohen, S. A.; Bercaw, J. E. *Organometallics* **1985**, *4*, 1006.

Scheme 1

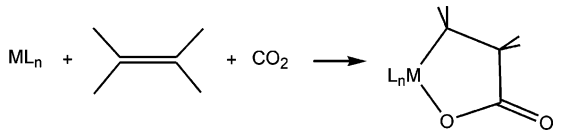

1). These compounds, also referred to as metalla-lactones, could be isolated and further be used to produce unsaturated carboxylic acids.[14−21] Ethylene complexes of Mo and W were also shown to react with CO_2, and quite remarkably, the reactions yielded acrylate derivatives.[22−25]

The above studies have significantly contributed to the understanding of the role of metal centers in catalytic CO_2 activation; however, our knowledge about the pathways toward the target molecules (and also to the undesired side products) is still fairly limited. Recent advances made in the application-oriented quantum chemistry provide a complementary methodology along these lines. Several organometallic reactions of synthetic importance have already been investigated from the theoretical side,[26,27] and these computational studies proved to be quite useful in elucidating the fundamental steps in catalytic processes. Here, we follow this approach and investigate the elementary steps of a reaction that involves transition-metal-mediated C−C coupling between the CO_2 and C_2H_4 molecules.

The reaction we have chosen was first described by Carmona et al.,[22−24] who found that bis(ethylene) complexes of Mo and W (*trans*-M$(C_2H_4)_2(PMe_3)_4$) afford binuclear hydrido-acrylates when reacted with CO_2, in which the two metal centers are linked via bridging acrylate ligands (see Scheme 2). This reaction is of particular interest because it incorporates two very important ingredients of CO_2 related catalytic synthesis: namely, the C−C coupling between CO_2 and an olefin, and the C−H bond cleavage that allows the formation of a C═C bond in the carboxylated species. Similar to our previous theoretical studies focusing on the reactions of bare transition metal atoms with CO_2,[28−32] we apply density functional theory in the present work and locate relevant stationary points on model potential energy surfaces associated with the reaction. Although our primary motivation was to understand the details of the coupling mechanism, we have investigated the subsequent elementary steps as well and explored the entire reaction path toward the hydrido-acrylate product.

To our knowledge, there are only a few theoretical studies addressing the issue of C−C coupling between CO_2 and unsaturated hydrocarbons.[33−37] These studies have focused on the structure of the Mo$(C_2H_4)_2(CO_2)(PMe_3)_3$ complex,[33] on the coordination modes of the CO_2 and the C_2H_4 ligands in $L_2Ni(CO_2)$ and $L_2Ni(C_2H_4)$ type model complexes,[34,35] and the CO_2−acetylene coupling mechanism.[36,37] Based on their ab initio CASSCF calculations, Dedieu et al. suggested that the CO_2−C_2H_4 coupling at NiL_2 centers involves a coordinated CO_2 attacked by an incoming C_2H_4 molecule.[34,35] On the other hand, CISD calculations carried out by Sakaki et al.[36,37] indicated that the five-membered nickelacycle species in the Ni(0) + CO_2 + C_2H_2 reaction is formed from an $NiL(CO_2)(C_2H_2)$ complex. The question of whether the coordination of both reacting ligands is a prerequisite for the CO_2−alkene coupling has recently been raised again (see Chapter 4 in ref 8), but still it remains unanswered.

In the present work, we clearly establish the intermediacy of the metalla-lactone species in the reaction depicted in Scheme 2 and we show that this intermediate is reached from a precursor complex that involves coordinated CO_2 and C_2H_4 ligands via a relatively low energy activation barrier. We also follow the fate of the metalla-lactone intermediate along the route toward the hydrido-acrylate product and give a detailed account of the elementary steps of the entire reaction.

In what follows in our paper, we first summarize the experimental evidence available for the investigated reaction, which guided our strategy in exploring possible reaction routes on a rather complicated potential energy surface. The molecular models and the technical details of our calculations are introduced next. In the discussion section, we first identify the elementary steps of the reaction and then we discuss the general features of the entire reaction pathway. A few points regarding the model construction (solvation effects and the issue of model truncation) are also discussed.

2. Experimental Evidence and Proposed Reaction Mechanism

As described in the original report,[22] the reactions of the *trans*-M$(C_2H_4)_2(PMe_3)_4$ complexes (M = Mo and W) with CO_2 were carried out in solution (in diethyl ether) under mild conditions (1 atm, room temperature or below). The new compounds, the μ-$(CH_2$═CH−$COO)_2[HM(C_2H_4)(PMe_3)_2]_2$ binuclear hydrido-acrylate complexes formed in these reactions, were first characterized by means of analytical, IR, and NMR data, and their structures were determined by single-crystal X-ray and neutron diffraction measurements.[22,23] These structural data served as a reference to evaluate the accuracy of the applied computational methodology regarding our structural predictions.

There is a solid body of evidence for a facile dissociation of a PMe_3 ligand from the *trans*-M$(C_2H_4)_2(PMe_3)_4$ complexes

(19) Hoberg, H.; Peres, Y.; Milchereit, A. *J. Organomet. Chem.* **1986**, *307*, C38.
(20) Hoberg, H.; Jemni, K.; Angermund, K.; Krüger, C. *Angew. Chem., Int. Ed. Engl.* **1987**, *26*, 153.
(21) Hoberg, H.; Peres, Y.; Krüger, C.; Tsay, Y. *Angew. Chem., Int. Ed. Engl.* **1987**, *26*, 771.
(22) Alvarez, R.; Carmona, E.; Cole-Hamilton, D. J.; Galindo, A.; Gutiérrez-Puebla, E.; Monge, A.; Poveda, M. L.; Ruiz, C. *J. Am. Chem. Soc.* **1985**, *107*, 5529.
(23) Alvarez, R.; Carmona, E.; Galindo, A.; Gutiérrez, E.; Marin, J. M.; Monge, A.; Poveda, M. L.; Ruiz, C.; Savariault, J. M. *Organometallics* **1989**, *8*, 2430.
(24) Galindo, A.; Pastor, A.; Pérez, P. J.; Carmona, E. *Organometallics* **1993**, *12*, 4443.
(25) Collazo, C.; del Mar Conejo, M.; Pastor, A.; Galindo, A. *Inorg. Chim. Acta* **1998**, *272*, 125.
(26) For relevant reviews, see: (a) Niu, S.; Hall, M. B. *Chem. Rev.* **2000**, *100*, 353. (b) Torrent, M.; Solà, M.; Frenking, G. *Chem. Rev.* **2000**, *100*, 439. (c) Dedieu, A. *Chem. Rev.* **2000**, *100*, 543.
(27) For representative examples from recent mechanistic studies, see: (a) Tobisch, S.; Ziegler, T. *J. Am. Chem. Soc.* **2002**, *124*, 4881. (b) Musashi, Y.; Sakaki, S. *J. Am. Chem. Soc.* **2002**, *124*, 7588. (c) Nakamura, E.; Yoshikai, N.; Yamanaka, M. *J. Am. Chem. Soc.* **2002**, *124*, 7181. (d) Aggarwal, V. K.; Harvey, J. N.; Richardson, J. *J. Am. Chem. Soc.* **2002**, *124*, 5747.
(28) Galan, F.; Fouassier, M.; Tranquille, M.; Mascetti, J.; Papai, I. *J. Phys. Chem. A* **1997**, *101*, 2626.
(29) Papai, I.; Mascetti, J.; Fournier R. *J. Phys. Chem. A* **1997**, *101*, 4465.
(30) Mascetti, J.; Galan, F.; Papai, I. *J. Coord. Chem. Rev.* **1999**, *190*−*192*, 557.
(31) Papai, I.; Hannachi, Y.; Gwizdala, S.; Mascetti, J. *J. Phys. Chem. A* **2002**, *106*, 4181.
(32) Papai, I.; Schubert, G.; Hannachi, Y.; Mascetti, J. *J. Phys. Chem. A* **2002**, *106*, 9551.
(33) Branchadell, V.; Dedieu, A. *Inorg. Chem.* **1987**, *26*, 3966.
(34) Dedieu, A.; Ingold, F. *Angew. Chem., Int. Ed. Engl.* **1989**, *28*, 1694.
(35) Dedieu, A.; Bo, C.; Ingold, F. In ref 4, p 23.
(36) Sakaki, S.; Mine, K.; Taguchi, D.; Arai, T. *Bull. Chem. Soc. Jpn.* **1993**, *66*, 3289.
(37) Sakaki, S.; Mine, K.; Hamada, T.; Arai, T. *Bull. Chem. Soc. Jpn.* **1995**, *68*, 1873.

Scheme 2

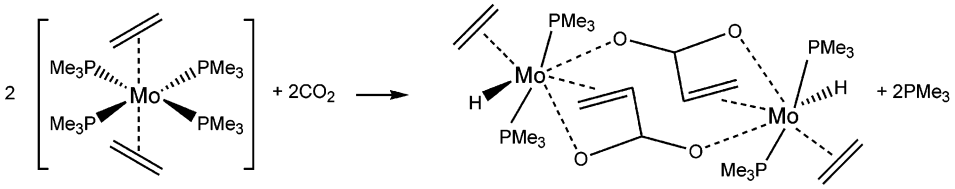

Scheme 3

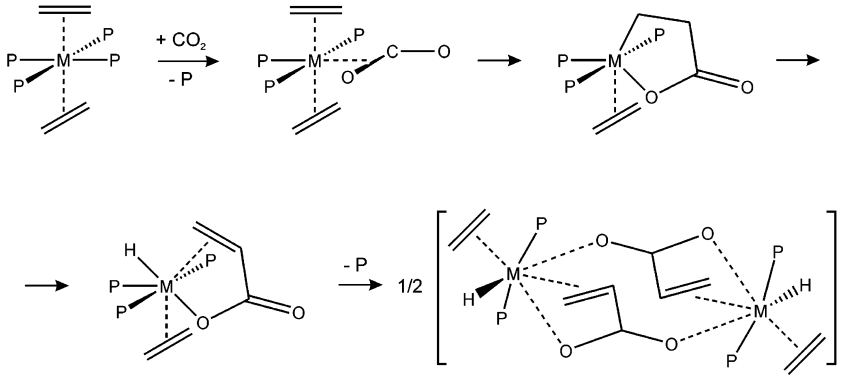

creating a vacant coordination site at the metal center, which can be saturated by other ligands.[22−24,38−44] For instance, the *trans*,*mer*-$M(C_2H_4)_2(N_2)(PMe_3)_3$ and *trans*,*mer*-$M(C_2H_4)_2(CO)(PMe_3)_3$ complexes can readily be prepared in solution.[38,39] Based on these findings, it has been presumed that the present coupling reaction is initiated by the replacement of a PMe_3 ligand by CO_2, but the intermediacy of a "mixed" $C_2H_4-CO_2$ complex (i.e., *trans*,*mer*-$M(C_2H_4)_2(CO_2)(PMe_3)_3$) has not been directly demonstrated experimentally.

A few scenarios for the C−C coupling step have also been outlined by Carmona et al.,[22,23] of which the oxidative coupling of CO_2 with C_2H_4 was suggested to be the most conceivable pathway giving rise to a five-membered metalla-lactone intermediate ($M(CH_2CH_2-COO)(C_2H_4)(PMe_3)_3$). The C−H bond was assumed to be cleaved in a subsequent β-hydrogen transfer to the metal center generating the hydrido-acrylate ($HM(CH_2=CH-COO)(C_2H_4)(PMe_3)_3$) species, which could then dimerize provided that an additional PMe_3 ligand is detached from each monomer.

The suggested elementary steps of the reaction are summarized in Scheme 3. We have investigated each step for M = Mo in the present work and located the intermediates and the connecting transition state structures on model potential energy surfaces. It was our intention in our study to provide a theoretical basis for the above picture.

3. Models and Computational Details

Two different molecular models have been considered in our study. The simpler model corresponds to complexes with PH_3 ligands, and the other involves the actual PMe_3 phosphines. We first searched for stationary points relevant to Scheme 3 using the smaller model and carried out normal coordinate analysis for the optimized structures to verify the nature of the stationary points. For each transition state structure, we calculated the intrinsic reaction coordinate (IRC) routes in both directions toward the corresponding minima. For some of the transition states, the IRC calculations failed to reach the energy minima on the potential energy surface; therefore, in those cases we carried out geometry optimizations from the beginning of the IRC path (pseudo-IRC calculations).

We assume that the entire reaction evolves on a single potential energy surface associated with the closed-shell singlet electronic ground states of the reactants and the hydrido-acrylate product. The relevance of this assumption was monitored by the inspection of the HOMO−LUMO gap for the stationary points, and it was also explicitly checked for various stages of the reaction by carrying out single-point energy calculations for the triplet states of all located stationary points. The latter calculations showed that the triplet states of the stationary points were always clearly above the corresponding singlet states (the calculated singlet−triplet splitting ranges between 20 and 70 kcal/mol). For structures exhibiting the lowest singlet−triplet energy separations, we carried out full geometry optimizations for their triplet states, but the relaxed triplet structures always remained above those of the singlet states. All of these calculations were performed at the B3LYP/SDDP level of density functional theory[45−47] using the Gaussian 98 program,[48] where SDDP refers to a basis set including the Stuttgart−Dresden relativistic small core ECP basis set[49] for Mo and the Dunning/Huzinaga DZ + polarization all electron basis set[50−52] for the lighter atoms.

(38) Carmona, E.; Marín, J. M.; Poveda, M. L.; Atwood, J. L.; Rogers, R. D. *J. Am. Chem. Soc.* **1983**, *105*, 3014.
(39) Carmona, E.; Galindo, A.; Poveda, M. L.; Rogers, R. D. *Inorg. Chem.* **1985**, *24*, 4033.
(40) Carmona, E.; Galindo, A.; Marín, J. M.; Gutiérrez, E.; Monge, A.; Ruiz, C. *Polyhedron* **1988**, *7*, 1831.
(41) Carmona, E.; Galindo, A.; Monge, A.; Muñoz, M. A.; Poveda, M. L.; Ruiz, C. *Inorg. Chem.* **1990**, *29*, 5074.
(42) Pastor, A.; Galindo, A. *J. Chem. Soc., Dalton Trans.* **1997**, 3749.
(43) Pastor, A.; Galindo, A.; Gutiérrez-Puebla, E.; Monge, A. *J. Organomet. Chem.* **1998**, *566*, 211.
(44) Mealli, C.; Masi, D.; Pastor, A.; Galindo, A. *J. Organomet. Chem.* **1998**, *569*, 21.
(45) Becke, A. D. *J. Chem. Phys.* **1993**, *98*, 5648.
(46) Lee, C.; Yang, W.; Parr, R. G. *Phys. Rev. B* **1988**, *37*, 785.
(47) Stephens, P. J.; Devlin, F. J.; Chabalowski, C. F.; Frisch, M. J. *J. Phys. Chem.* **1994**, *98*, 11623.
(48) Frisch, M. J.; Trucks, G. W.; Schlegel, H. B.; Scuseria, G. E.; Robb, M. A.; Cheeseman, J. R.; Zakrzewski, V. G.; Montgomery, J. A.; Stratmann, R. E.; Burant, J. C.; Dapprich, S.; Millam, J. M.; Daniels, A. D.; Kudin, K. N.; Strain, M. C.; Farkas, Ö.; Tomasi, J.; Barone, V.; Cossi, M.; Cammi, R.; Mennucci, B.; Pomelli, C.; Adamo, C.; Clifford, S.; Ochterski, J.; Petersson, G. A.; Ayala, P. Y.; Cui, Q.; Morokuma, K.; Malick, D. K.; Rabuck, A. D.; Raghavachari, K.; Foresman, J. B.; Cioslowski, J.; Ortiz, J. V.; Stefanov, B. B.; Liu, G.; Liashenko, A.; Piskorz, P.; Komáromi, I.; Gomperts, R.; Martin, R. L.; Fox, D. J.; Keith, T.; Al-Laham, M. A.; Peng, C. Y.; Nanayakkara, A.; Gonzalez, C.; Challacombe, M.; Gill, P. M. W.; Johnson, B.; Chen, W.; Wong, M. W.; Andres, J. L.; Head-Gordon, M.; Replogle, E. S.; Pople, J. A. *Gaussian 98*, revision A.9; Gaussian, Inc.: Pittsburgh, PA, 1998.
(49) Dolg, M.; Stoll, H.; Preuss, H.; Pitzer, R. M. *J. Phys. Chem.* **1993**, *97*, 5852.
(50) Dunning, T. H., Jr. *J. Chem. Phys.* **1970**, *53*, 2823.

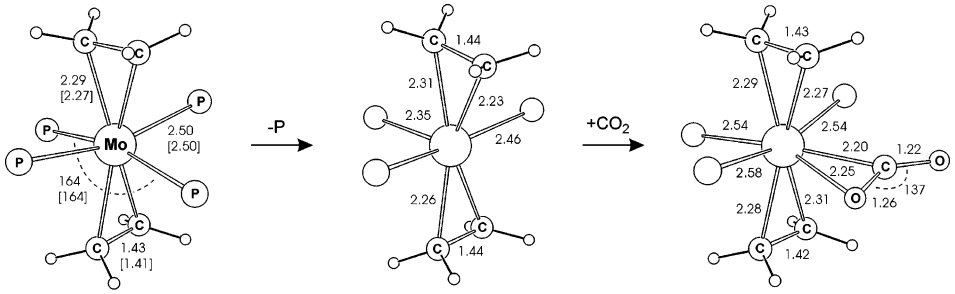

1 **1'** **2**

Figure 1. Optimized structures and selected geometric parameters of complexes involved in the PMe_3/CO_2 substitution (bond lengths in angstroms, angles in degrees; experimental structural parameters of complex **1** are shown in brackets).

The structures obtained in these calculations were used to construct the larger models by substituting the PH_3 ligands with PMe_3 groups. The ADF package[53] was then used to obtain optimized geometries for the minima and transition states of the larger model (geometry optimizations for the $PR_3 = PMe_3$ models at the B3LYP/SDDP level are not feasible with our present computer facilities). These calculations were carried out by using the BP86[54,55] density functional along with the standard triple-ζ polarization Slater-type orbital (STO) basis set for Mo (database IV in ADF) and the double-ζ polarization set (database III) for the remaining atoms. The frozen core approximation was applied for the Mo(1s−3d) and P(1s−2p) inner shells and also for the 1s shells of the C and O atoms. First-order quasi-relativistic corrections[56−58] were also included in these calculations.

As a next step, single-point energy calculations were carried out at the B3LYP/SDDP level for the structures obtained with the larger model. These later results will be used throughout the paper to discuss the energetics of the gas-phase reaction. To take into account the effect of the solvent medium, we applied the polarized continuum model (PCM)[59] as implemented in Gaussian 98 and carried out reaction field calculations for the structures optimized in the gas phase.The dielectric constant of the polarizable medium was set to $\epsilon = 4.33$ so as to simulate diethyl ether used in the experiments.

4. Results and Discussion

We start our discussion by presenting the structure and relative stability of the located stationary points starting from the initial reactant complex and tracing the elementary steps along the reaction pathway. Unless otherwise stated, the reported data will be those calculated for the $PR_3 = PMe_3$ model and the energies will refer to the gas-phase calculations. The solvent effects and the issue of model simplification will be discussed later in sections 4.6 and 4.8. For clarity of the figures, we report only the most relevant structural parameters; however, the Cartesian coordinates of all optimized structures are provided in the Supporting Information.

4.1. Phosphine Substitution. The optimized structures of the three complexes involved in the stepwise phosphine substitution[60] occurring at the initial stage of the reaction are depicted in Figure 1. The parent tetraphosphine complex (**1**) has a distorted octahedral structure with the four phosphines displaced along the equatorial plane and the two ethylenes in the *trans*-staggered position typical of bis(ethylene) metal complexes.[61] The distortion refers to the deviation of the P−Mo−P angle of the trans phosphines from 180°, which is due to steric repulsion operating between the methyl groups of adjacent phosphines and also between the C_2H_4 and PMe_3 ligands.

We have recently shown[62] that the experimentally characterized structure of the $M(C_2H_4)_2(PMe_3)_4$ complexes (M = Mo, W) can only be properly reproduced if the actual PMe_3 ligands are considered in the calculations. For the simplified model, the calculations gave too short M−P bond distances and the experimentally observed ruffled arrangement of the phosphine ligands was not seen either. The discrepancy was interpreted in terms of different steric interactions between the PH_3 and PMe_3 ligands in their square-planar arrangement about the Mo center. This argument was further supported by the computed phosphine dissociation energies because the calculations carried out with the large model predicted low dissociation energies (4−11 kcal/mol for M = Mo, depending on the applied methodology), whereas the application of the $PR_3 = PH_3$ model gave much higher values (around 25 kcal/mol). In line with these results, our present B3LYP/SDDP calculations predict 22.9 and 6.4 kcal/mol for the PH_3 and PMe_3 dissociation energies, respectively.

It appears from these results that the replacement of the bulky PMe_3 group by PH_3 is a rather crude approximation because the steric interactions are not properly described with the small model (see also ref 63). Nevertheless, we decided to use the simpler model as well, first to find reasonable initial structures for the larger models and also to keep the most demanding parts of the computations (vibrational analysis, IRC following calculations) within reasonable bounds.

The dissociation of a PMe_3 ligand from **1** leads to the unsaturated $Mo(C_2H_4)_2(PMe_3)_3$ complex (**1′**) in which the steric congestion is significantly reduced as indicated by the structural

(51) Dunning, T. H., Jr.; Hay, P. J. *Methods of Electronic Structure Theory*; Schaefer, H. F., III., Ed.; Plenum Press: New York, 1977; Vol. 3.
(52) Schaefer, H. F., III. *J. Chem. Phys.* **1985**, *83*, 5721.
(53) ADF2000.02, SCM, Theoretical Chemistry, Vrije Universiteit, Amsterdam, The Netherlands, http://www.scm.com.
(54) Becke, A. D. *Phys. Rev. A* **1988**, *38*, 3098.
(55) Perdew, J. P. *Phys. Rev. B* **1986**, *33*, 8822.
(56) Snijders, J. G.; Baerends, E. J.; Ros, P. *Mol. Phys.* **1979**, *38*, 1909.
(57) Boerrigter, P. M.; Baerends, E. J.; Snijders, J. G. *Chem. Phys.* **1988**, *122*, 357.
(58) Ziegler, T.; Tschinke, V.; Baerends, E. J.; Snijders, J. G.; Ravenek, W. *J. Phys. Chem.* **1989**, *93*, 3050.
(59) Miertus, S.; Scrocco, E.; Tomasi, J. *Chem. Phys.* **1981**, *55*, 117.
(60) The alternative concerted mechanism of the PMe_3/CO_2 substitution is unlikely because the coordination of CO_2 is prohibited by the steric hindrance of the PMe_3 ligands.
(61) (a) Siegbahn, P. E. M.; Brandemark, U. B. *Theor. Chim. Acta* **1986**, *69*, 110. (b) Bernardi, F.; Bottoni, A.; Calcinari, M.; Rossi, I.; Robb, M. A. *J. Phys. Chem. A* **1997**, *101*, 6310. (c) Tlenkopatchev, M.; Fomine, S. *J. Organomet. Chem.* **2001**, *630*, 157. (d) Handzlik, J.; Hartl, F.; Szymańska-Buzar, T. *New J. Chem.* **2002**, *26*, 145.
(62) del Rio, D.; Schubert, G.; Pápai, I.; Galindo, A. *J. Organomet. Chem.* **2002**, *663*, 83.
(63) Hascall, T.; Rabinovich, D.; Murphy, V. J.; Beachy, M. D.; Friesner, R. A.; Parkin, G. *J. Am. Chem. Soc.* **1999**, *121*, 11402.

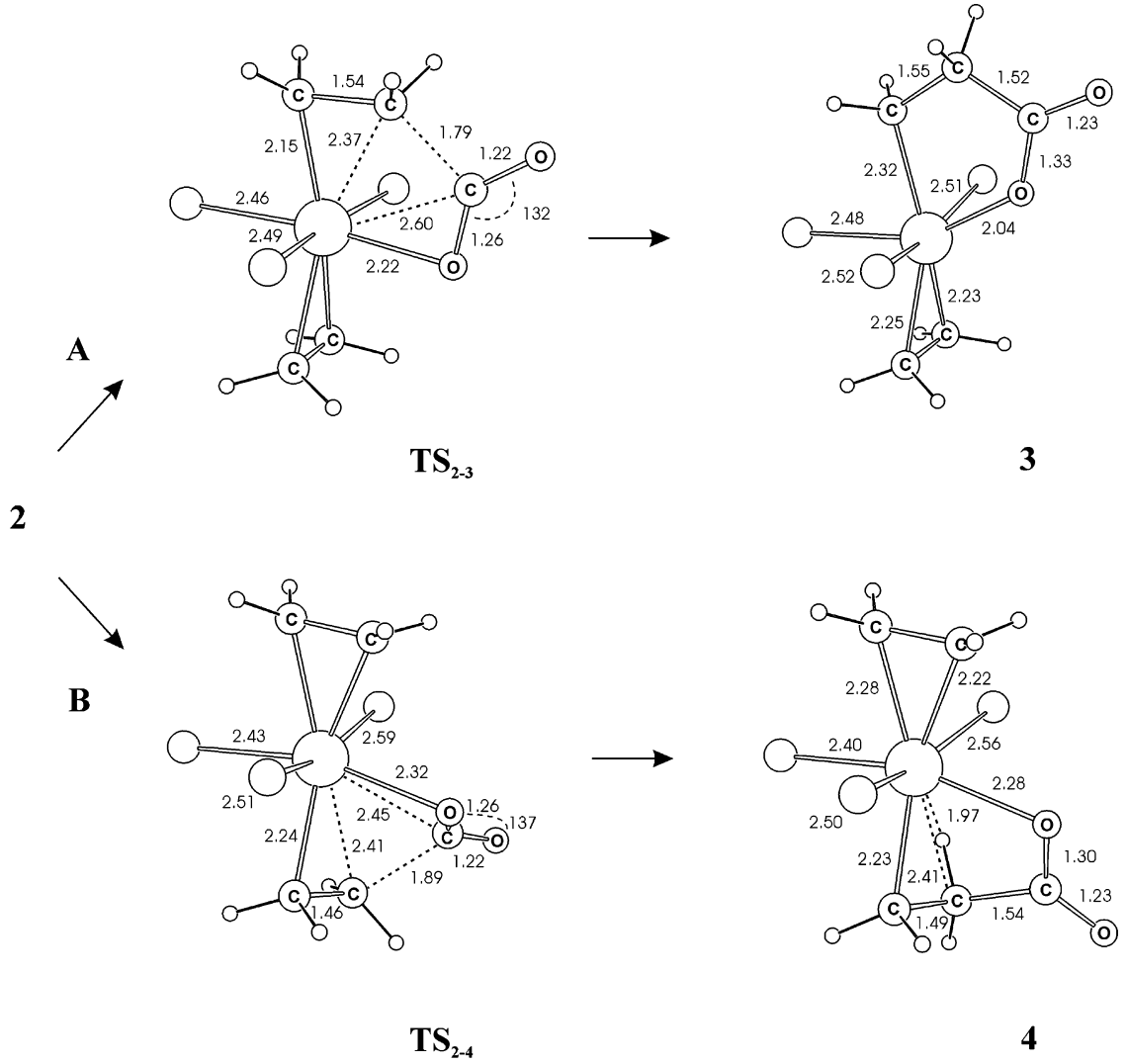

Figure 2. Optimized structures and selected geometric parameters of complexes and transition states involved in the $CO_2-C_2H_4$ coupling process.

changes found in the coordination sphere; in particular, the Mo−P bonds are notably shortened, the C_2H_4 ligands shift to the vacant site, and so forth (for a detailed description, see ref 62). The vacant site in **1′** allows the coordination of a CO_2 molecule to the metal center resulting in the hypothetical Mo$(C_2H_4)_2(CO_2)(PMe_3)_3$ intermediate (**2**). In this complex, the η^2_{CO}-coordinated CO_2 is aligned with the equatorial plane and the two C_2H_4 ligands keep their staggered orientation. As pointed out before by Branchadell and Dedieu,[33] this structure corresponds to the optimal interaction of the metal d_π orbitals with the π^* orbitals of the three π-acceptor ligands since three orthogonal d_π orbitals are involved in the stabilizing metal−ligand back-donation mechanism. The formation of the Mo−CO_2 bond has an appreciable impact on the entire coordination sphere, in particular, on the strength of the metal−phosphine bonds (see the variation of Mo−P distances in Figure 1).

The binding energy of CO_2 in **2** is predicted to be 6.2 kcal/mol, which is practically identical to that of a PMe_3 ligand in **1** indicating that the dissociative interchange of the PMe_3 and CO_2 ligands is both thermodynamically and kinetically allowed.

4.2. $CO_2-C_2H_4$ Coupling. Considering the equilibrium structure of complex **2**, one can envision two alternative C−C coupling channels. Hereafter, route A will denote the coupling with the C_2H_4 having its C−C axis aligned nearly perpendicular to the coordinated C−O, whereas the coupling with the other C_2H_4 (lying nearly parallel with C−O) will be referred to as route B (see Figure 2). This consideration is, of course, based on a static picture. NMR studies show a fluxional behavior of complex **1** at room temperature (see refs 38, 39) which is attributed to the fast conrotatory motion of the ethylenes around the molecular axes. Nevertheless, we use this picture as a tool to locate possible transition states for the $CO_2-C_2H_4$ coupling mechanism.

The intermediate formed on route A (**3**) involves a nearly planar five-membered metallacycle as illustrated by two small dihedral angles (ϕ(MoC$^\alpha$C$^\beta$C^O) = 8°, ϕ(C$^\alpha$C$^\beta$C^{O}O) = 9°), and the metallacycle is perpendicular to the nonreacting ethylene. We predict **3** to be very close in energy to **2** (within 1 kcal/mol), and the activation barrier for the C−C coupling is only 12 kcal/mol. The C−C coupling on route B yields a metallacycle as well; however, the structure of this intermediate (**4**) is rather different from that of **3** (see Figures 2 and 3). The most apparent difference is the presence of an agostic interaction between the Mo atom and one of the C−H bonds at the β position of the chelating CH_2CH_2COO moiety, but some differences in the relative strength of the Mo−C$^\alpha$ and Mo−O bonds in **3** and **4** can also be observed, as judged from the corresponding bond distances. The metallacycle in **4** is significantly distorted

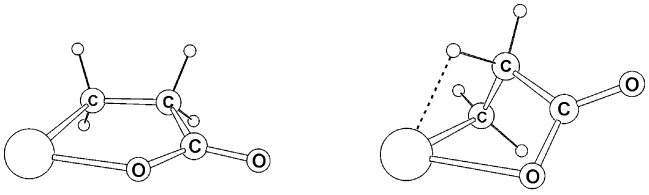

3 4

Figure 3. Structure of the metallacycles in intermediates **3** and **4**.

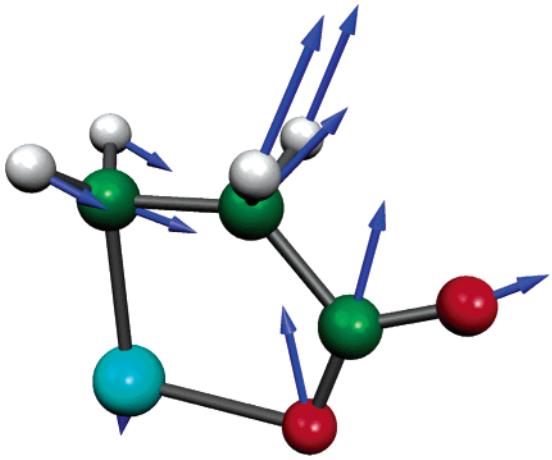

Figure 4. Vector representation of the normal coordinate corresponding to the imaginary frequency of $\mathbf{TS_{2-3}}$ (ancillary ligands are omitted for clarity).

($\phi(MoC^{\alpha}C^{\beta}C^{O}) = 80°$, $\phi(C^{\alpha}C^{\beta}C^{O}O) = 53°$). The presence of the agostic interaction is clearly indicated by the typically short Mo−H and Mo−C^{β} bond distances (1.97 and 2.41 Å, respectively) and also by the vibrational frequency calculated for the agostic C−H stretching mode (2494 cm^{-1}, as computed for the small model). The agostic intermediate is predicted to be 5 kcal/mol less stable than **3**. Moreover, the activation barrier of the **2** → **4** pathway is notably higher (22 kcal/mol) than the value obtained for route A, showing that the later channel is also kinetically less favorable.

The formation of the C−C bond in route A occurs via a five-center transition state ($\mathbf{TS_{2-3}}$), and the normal vector corresponding to the imaginary vibrational frequency (see Figure 4) indicates that the C−C bond formation is strongly coupled with the cleavage of the associated Mo−C bonds. The weakening of these bonds in $\mathbf{TS_{2-3}}$ is apparent from their elongation as compared to those in **2**. The C−C bond of the ethylene is lengthened as well, which is associated with the weakening of the C−C π bond.

To monitor the structural changes occurring in the **2** → $\mathbf{TS_{2-3}}$ → **3** CO_2−C_2H_4 coupling process, we plotted the energy variation and a few characteristic structures along the pseudo-IRC route (Figure 5). These calculations indicate that the C−C bond formation proceeds via the CO_2 attack on the proximal carbon atom of C_2H_4. The approach of the CO_2 ligand is initiated by its rotation to become coplanar with the molecular axis of the reacting ethylene, and the C−C coupling occurs in the planar arrangement.

In the $\mathbf{TS_{2-4}}$ transition state, the reacting ligands are nearly coplanar ($\phi(C^{\alpha}C^{\beta}C^{O}O) = 8°$), but in contrast to $\mathbf{TS_{2-3}}$, the metal center is not positioned in this plane. The planarity of the CH_2-CH_2COO moiety is preserved until the C^{β}−C^{O} bond formation is accomplished, but then the carboxyl group rotates around the C^{β}−C^{O} bond. This rearrangement is driven by the strengthening of the Mo−O bond, and the five-membered metallacycle is further stabilized by twisting of the β-CH_2 group to allow for the Mo···H−C agostic interaction.

The most characteristic molecular orbital (corresponding to HOMO-2) of the $\mathbf{TS_{2-3}}$ transition state is presented in Figure 6, and it clearly illustrates the role of the metal atom in the C−C coupling process. This orbital shows a close resemblance to that described by Sakaki and co-workers[36,37] for the Ni(0) + CO_2 + C_2H_2 → oxanickela-cyclopentene coupling reaction in that it is a linear combination of Mo $4d_{\pi}$ and the π^* orbitals of the reacting ligands. This combination corresponds to simultaneous Mo → CO_2 and Mo → C_2H_4 electron donation and C−C bonding interactions between CO_2 and C_2H_4. After passing the transition state, this orbital gradually loses its Mo 4d character and keeps its C^{β}−C^{O} bonding nature. The population analysis carried out for the stationary points of the two coupling channels shows that a notable amount of negative charge is transferred from Mo to the ligands involved in the coupling,[64] which is consistent with the notion of oxidative coupling used generally to characterize the CO_2−olefin coupling process.

4.3. Alternative Route to the Agostic Intermediate. Our calculations suggest that the CO_2−C_2H_4 coupling proceeds via route A resulting in the metalla-lactone intermediate **3**. Due to the high activation barrier, the formation of the agostic complex **4** along the B coupling channel is prohibited at room temperature. However, structure **4** is a key reaction intermediate in the formation of the hydrido-acrylate complex in a subsequent phase of the reaction as shown in the following section. We have, therefore, explored possible low energy routes that connect intermediates **3** and **4**.

The **3** → **4** rearrangement may occur, for example, via intermediate **3″** (see Figure 7), which is a metalla-lactone species that can be derived formally from **3** by an internal rotation of the Mo(C_2H_4)(CH_2CH_2COO) core with respect to the equatorial plane of the phosphine ligands. Indeed, structure **3″** corresponds to a well-defined minimum on the potential energy surface lying about 4 kcal/mol above the original metalla-lactone complex (**3**). Intermediate **3″** can then readily transform to the agostic complex, because structure **4** is only 1 kcal/mol less stable than **3″** and the activation barrier represented by $\mathbf{TS_{3''-4}}$ is only 6 kcal/mol. This latter rearrangement involves the shift of the carboxylate group to the vacant coordination site in **3″** followed by the formation of the agostic interaction.

Concerning the **3** → **3″** transformation, we considered the possibility of a phosphine exchange process and found that the dissociation of a PMe_3 ligand from **3** requires an energy of only 10 kcal/mol to give an unsaturated biphosphine complex ($\mathbf{3'_d}$), which can bind another PMe_3 and form intermediate **3″**. The associative mechanism of the phosphine exchange appears to be less feasible, because the 18 electron Mo(C_2H_4)(CH_2CH_2-COO)(PMe_3)$_4$ species ($\mathbf{3'_a}$), although located as a minimum on the PR_3 = PMe_3 potential energy surface, is predicted to be an extremely weakly bound system with the present methodology.[65]

(64) For instance, the net atomic charge on Mo decreases from −0.68 to −0.13 when going from **2** to **3**, whereas the sum of net charges associated with the atoms of the reacting ligands vary from −0.32 to −0.50 (CO_2) and from −0.15 to −0.30 (C_2H_4) (these values are obtained from natural population analysis carried out for the PR_3 = PH_3 model; a similar trend is observed for the **2** → **4** coupling channel).

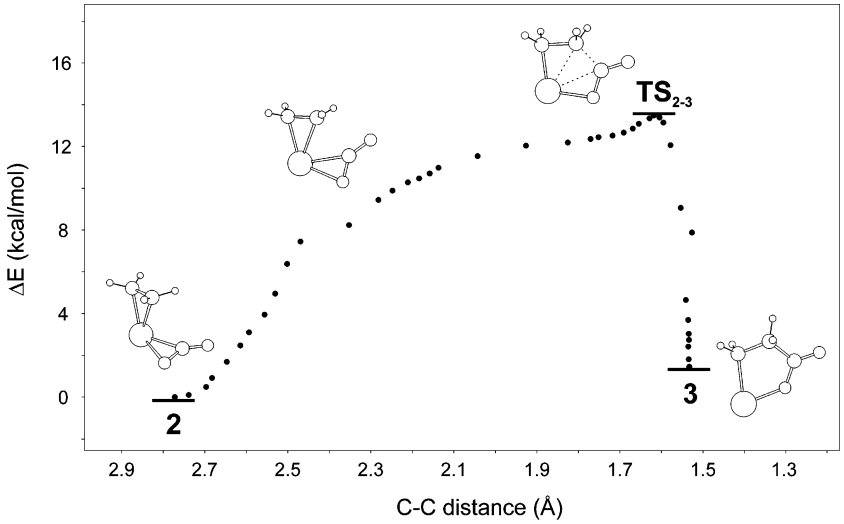

Figure 5. Energy variation with respect to the C−C distance measured between the carbon atoms involved in the C−C bond formation as obtained from pseudo-IRC calculations (see section 3; energies are given relative to structure **2**).

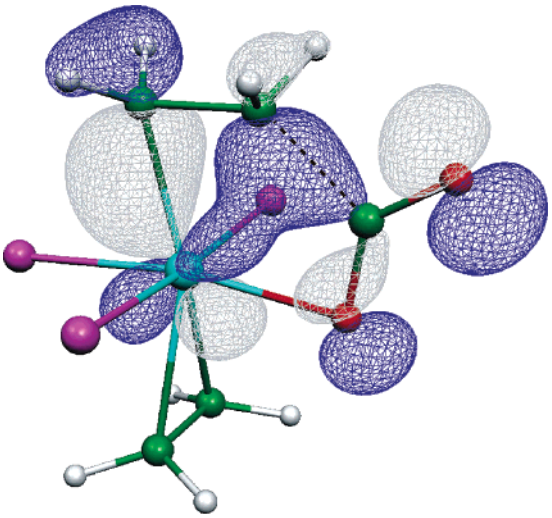

Figure 6. Surface plot of the molecular orbital (HOMO-2) corresponding to CO_2−C_2H_4 bonding interaction in $\mathbf{TS_{2-3}}$.

In an attempt to estimate the energy barrier for a possible **3** → **3″** internal rearrangement, we performed constrained geometry optimizations by varying the relative position of the $Mo(C_2H_4)(CH_2CH_2COO)$ and $Mo(PMe_3)_3$ units; however, no saddle points describing the internal rotation could be located. Another route corresponding to single ethylene rotation and subsequent deformation of the metallacycle part (as shown in Figure 3) was examined as well, but the 90° rotation of the C_2H_4 ligand in **3** (i.e., the eclipsed arrangement of C_2H_4 and the metallacycle) has turned out to be energetically unfavored (35 kcal/mol less stable than **3**).

These results indicate that the **3** → **4** transformation likely proceeds via the dissociative phosphine exchange mechanism, although the internal rearrangement cannot be completely excluded from consideration either. Because the overall energy barrier of the **3** → **4** transformation is at most 10 kcal/mol, we conclude that the formation of the agostic intermediate is kinetically more favorable from the metalla-lactone species than via the direct **2** → **4** C−C coupling path.

4.4. *β*-Hydrogen Transfer. The agostic intermediate **4** can undergo *β*-H transfer to form a hydrido-acrylate species **5** (see Figure 8). The hydrogen shift proceeds via the $\mathbf{TS_{4-5}}$ transition state, which lies 9 kcal/mol higher in energy than the agostic complex. The *β*-H transfer step is thermodynamically downhill because the hydrido-acrylate intermediate is predicted to be 5 kcal/mol more stable than **4**.

The structure of intermediate **5** can be characterized as a distorted pentagonal bipyramid, where the three phosphines, the hydride ligand, and one of the carboxylate oxygens of the acrylate group are in the equatorial plane, whereas the ethylene and the olefinic functionality of the acrylate coordinate in the apical positions. The acrylate group thus binds via its C═C and C−O functionalities to the metal atom. The olefinic part of the acrylate forms a standard metal-olefin *π*-bond with Mo, whereas the oxygen binds in a covalent M−O manner to the metal.

The relative position of the three phosphine ligands hardly changes in the *β*-H shift process; they keep their T-shape arrangement even in **5**, where the hydride ligand is displaced between two adjacent phosphines. The strength of the three Mo−P bonds, however, is rather different, as seen from their lengths. The longest Mo−P bond (2.59 Å) corresponds to PMe_3 being in a pseudo-trans position to the metal-hydride bond indicating a notable trans influence.

4.5. Hydrido-Acrylate Dimerization. The weakly bound PMe_3 can dissociate from **5** resulting in the $HMo(CH_2{=}CH{-}COO)(C_2H_4)(PMe_3)_2$ species (**5′**, see Figure 9). The energy required to dissociate this PMe_3 is calculated to be almost the same (10 kcal/mol) as that for the **3** → $\mathbf{3'_d}$ step. Intermediate **5′** may rearrange to structure **5″** by an internal rotation of the two olefinic ligands with respect to the $MoH(PMe_3)_2$ moiety. These two biphosphine complexes are close in energy (**5″** is only 2 kcal/mol more stable than **5′**), and the barrier of the rearrangement is very small (about 1 kcal/mol) indicating that the internal rotation can readily occur.

The distal O atom of the acrylate group in **5″** can coordinate to another Mo center allowing for a dimerization process that leads to the experimentally observed binuclear hidrido-acrylate complex (**6**; see Figure 9). The dimerization energy is calculated

(65) B3LYP/SDDP calculations carried out for the BP86/STO equilibrium geometries predict $\mathbf{3'_a}$ to be isoenergetic with **3** + PMe_3. Geometry optimization carried out for $\mathbf{3'_a}$ at the B3LYP/SDDP level yield rather elongated (2.73 Å) Mo−P bonds for the phosphines being coplanar with the metallacycle.

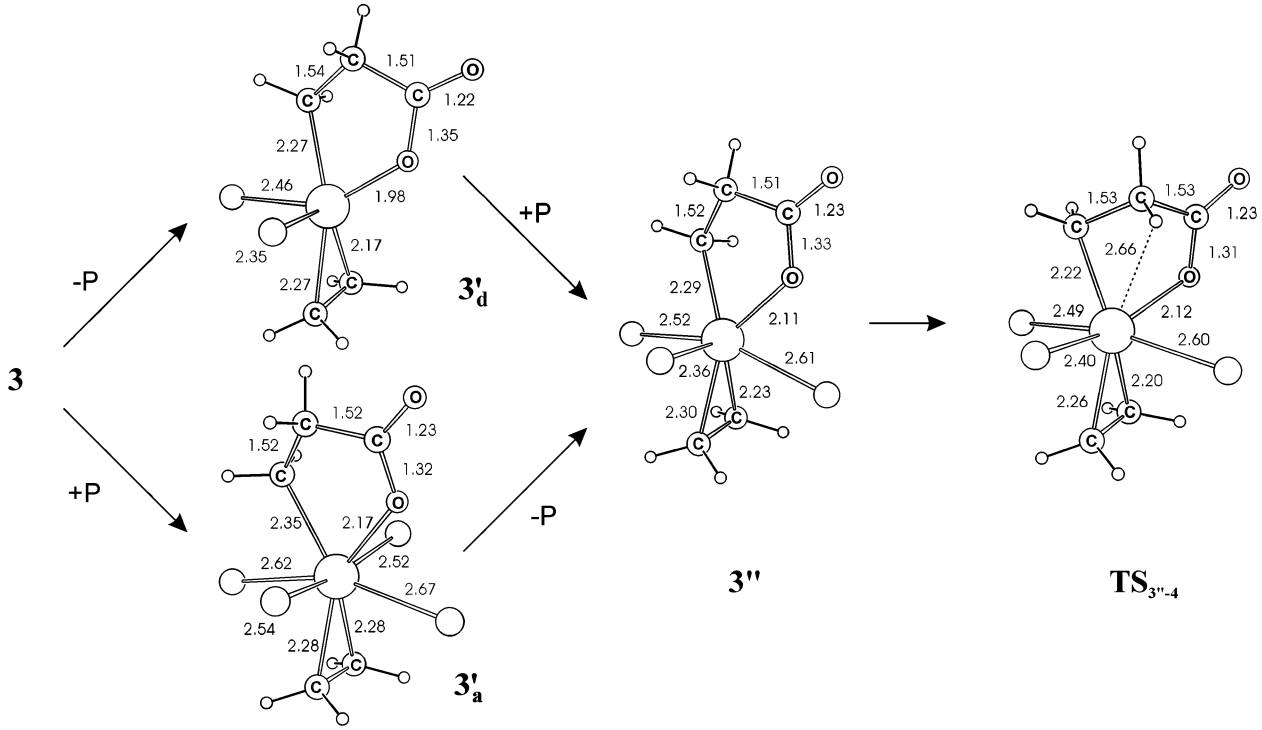

Figure 7. Optimized structures and selected geometric parameters of complexes and transition states involved in the **3** → **4** rearrangement.

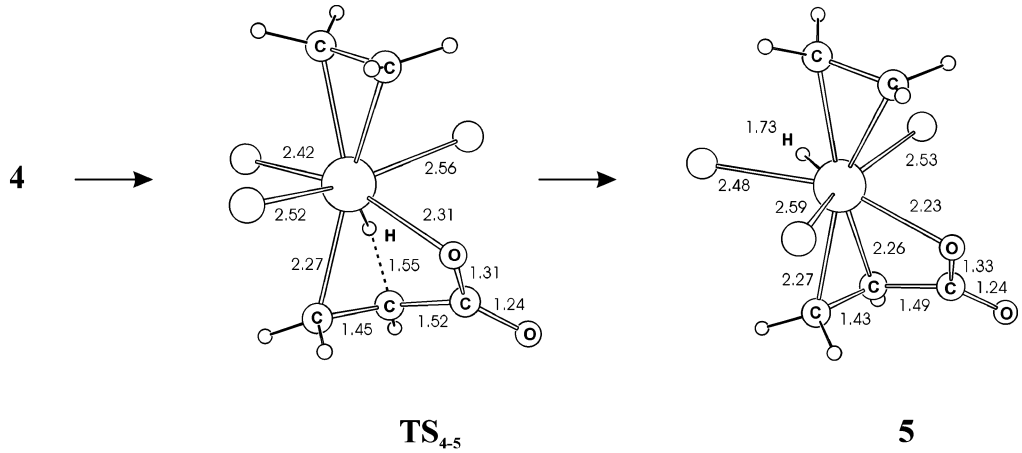

Figure 8. Optimized structures and selected geometric parameters of complexes and transition states involved in the β-hydrogen transfer process.

to be 38 kcal/mol; therefore, the last step of the reaction provides an important energy gain for the system. The dimerization induces only slight variations in the structure of the monomeric units. Notable effects can be observed only for the bridging carboxylate group (see the two C−O bond lengths in **5″** and **6**). It is interesting to mention that the two units in **6** are enantiomeric structures of complex **5″**, resulting in the heterochiral dimer. The chirality of the monomers is inherited from intermediate **2**, where the coordination of CO_2 yields two enantiomers. The dimerization between the same enantiomers cannot occur for steric reasons.

Our structural predictions for **6** are in full agreement with the structure determined from single-crystal X-ray measurements.[22,23] It is apparent from Figure 9 that the experimental structural parameters are well reproduced with the present methodology.

4.6. Overall Energetics, Solvent Effects. Having presented the structure of the located stationary points, we continue our discussion by summarizing the energetics of the entire reaction path. In Table 1, we collected the energy variations for the revealed elementary steps as computed on the $PR_3 = PH_3$ and $PR_3 = PMe_3$ model potential energy surfaces. The energy profile constructed from the gas-phase relative energies presented thus far (first column in Table 1) is shown in Figure 10. It is clearly seen that the transition state connecting the CO_2 complex (**2**) directly with the agostic intermediate (**4**) lies high above the other located transition states; therefore, route B can be conclusively ruled out as a possible $CO_2-C_2H_4$ coupling path and should not contribute to the rate of the coupling process.

We mention at this point that our calculations indicated notable internal charge polarization in most of the located intermediates and transition states (see calculated dipole moments in Table 1). Significant polarization occurs already in the **1′** + CO_2 → **2** coordination step due to the Mo → CO_2 charge transfer, which is carried over onto the subsequent intermediates and it becomes even more enhanced in the

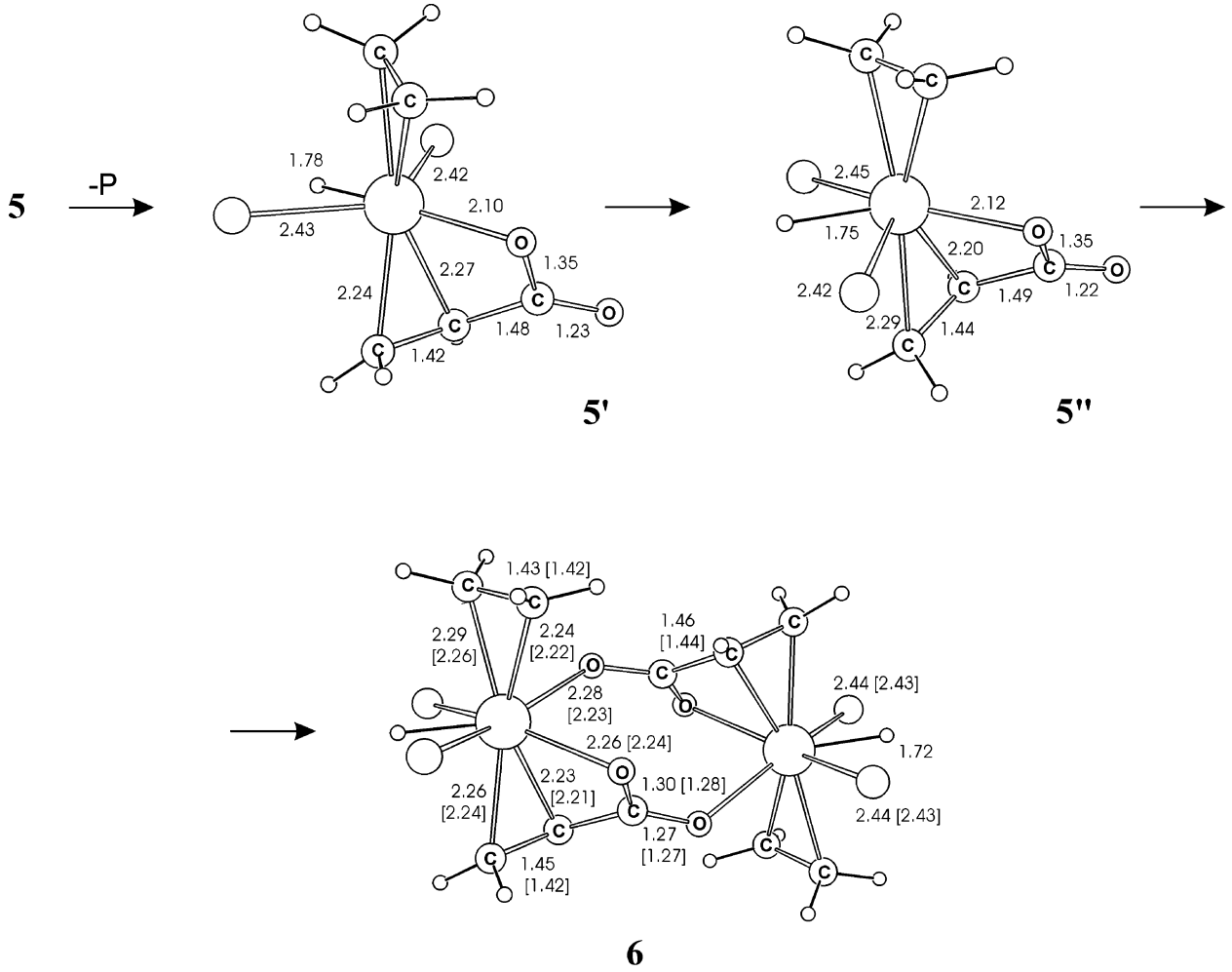

Figure 9. Optimized structures and selected geometric parameters of complexes and transition states involved in the dimerization process. Average experimental values from X-ray diffraction measurements for **6** are given in brackets.

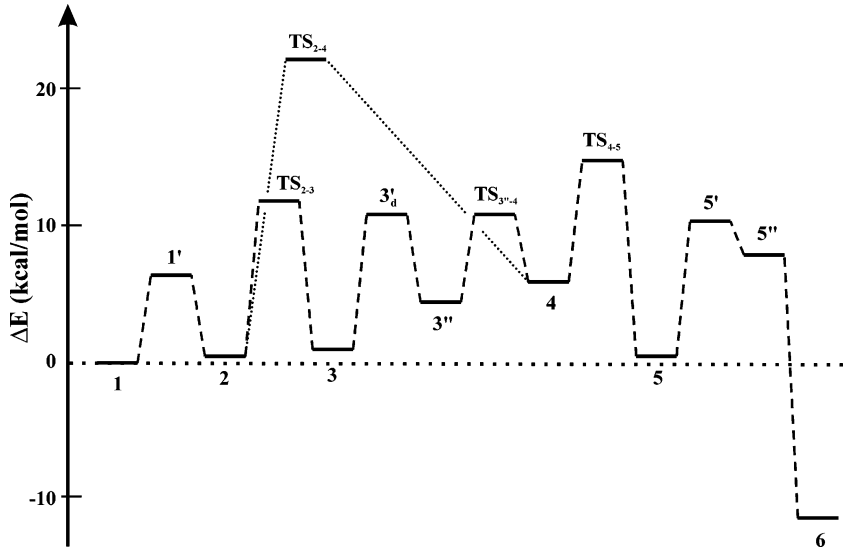

Figure 10. Energy profile of the entire reaction pathway corresponding to the gas-phase $PR_3 = PMe_3$ model (see first column in Table 1). Note that the reacting CO_2 molecule and the dissociating phosphine ligands are omitted from the notation of the elementary steps (the correct stoichiometry is provided in Table 1).

hydrido-acrylate species. For this reason, we found it important to incorporate solvation effects into the relative energies. So, before proceeding to discuss the energetics of the reaction, we introduce the results concerning the solvated model.

The solvation energies were estimated in terms of the PCM model as described in section 3, and the results are also given in Table 1. The energy profile corresponding to the solvated $PR_3 = PMe_3$ model is shown in Figure 11. The energy

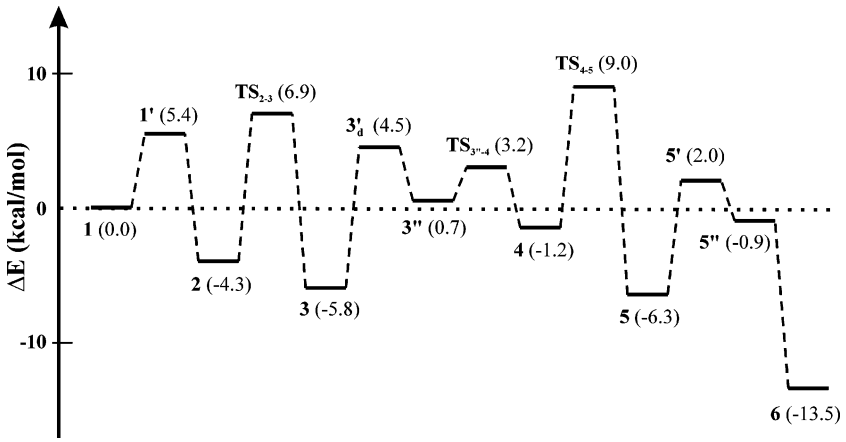

Figure 11. Energy profile corresponding to the solvated $PR_3 = PMe_3$ model (ΔE_s values are from Table 1).

Table 1. Summary of Relative Energies (in kcal/mol) along the Entire **1** + CO_2 → ($^1/_2$)·**6** + 2PMe_3 Reaction Path (the Reference Level Corresponds to **1** + CO_2 for Each Model[a])

	$PR_3 = PMe_3$				$PR_3 = PH_3$		
	ΔE_g	δE_s	ΔE_s	μ (D)	ΔE_g	ΔE_g^{ZPE}	$\Delta G°_g$
1 + CO_2	0.0	−1.6 (−0.9)	0.0	0.00	0.0	0.0	0.0
1′ + PR_3 + CO_2	6.4	−2.6 (−1.1)	5.4	0.80	22.8	20.4	9.8
2 + PR_3	0.2	−6.1 (−5.3)	−4.3	7.58	13.8	13.2	13.9
TS2–3 + PR_3	12.0	−6.7 (−5.9)	6.9	5.62	27.2	26.3	25.9
TS2–4 + PR_3	22.5	−5.2 (−4.4)	18.8	5.88	35.8	34.8	35.9
3 + PR_3	0.9	−8.3 (−7.5)	−5.8	7.87	15.2	15.3	15.0
3′d + 2PR_3	11.0	−7.2 (−6.4)	4.5	8.52	28.7	26.4	16.2
3″ + PR_3	4.7	−5.6 (−4.8)	0.7	6.84	22.3	23.3	23.6
TS3″–4 + PR_3	10.9	−9.2 (−8.4)	3.2	7.85	29.7	29.5	30.0
4 + PR_3	6.0	−8.7 (−7.9)	−1.2	7.81	27.1	27.0	27.7
TS4–5 + PR_3	14.9	−7.5 (−6.7)	9.0	7.72	38.9	36.5	37.2
5 + PR_3	0.6	−8.5 (−7.7)	−6.3	8.65	23.8	22.4	23.0
5′ + 2PR_3	10.7	−10.2 (−8.6)	2.0	9.22	36.6	32.0	21.8
5′ + 2PR_3	8.1	−10.6 (−9.0)	−0.9	9.19	33.5	29.2	19.4
($^1/_2$)·**6** + 2PR_3	−1.4	−5.8 (−2.1)	−13.5	1.43	10.0	7.4	5.5

[a] Notation: ΔE_g, relative energies in gas phase; δE_s, sum of the energy stabilization calculated for the components involved in a given step due to the presence of the $\epsilon = 4.33$ dielectric medium; the stabilization of the intermediate or transition state is given in parentheses (for CO_2 and PMe_3, these values are −0.7 and −0.8 kcal/mol, respectively); ΔE_s, relative energies including the solvent effects ($\Delta E_s = \Delta E_g + \delta E_s + 1.6$; the value of 1.6 is introduced to shift the reference level to **1** + CO_2); μ, dipole moments (absolute values) of the intermediates and transition states; ΔE_g^{ZPE}, relative energies corrected for ZPE (zero point energy) contributions ($PR_3 = PH_3$ model); $\Delta G°_g$, relative Gibbs free energies ($PR_3 = PH_3$ model).

stabilization of the intermediates and the transition states caused by the presence of the $\epsilon = 4.33$ dielectric medium typically varies between 4 and 9 kcal/mol, and in accordance with the calculated dipole moments, the effect is more important in the second half of the reaction path. Due to this stabilization, most of the reaction intermediates fall below the **1** + CO_2 reference level, which was not the case in the gas-phase calculations, and the highest lying transition state (**TS4–5**) is now only 9 kcal/mol above the reactants. Our results thus underline the importance of incorporating solvent effects in the calculation of relative energies,[66] and our further discussion will be based on the energy profile presented in Figure 11.[67]

4.7. Characteristic Features of the Reaction Path. We point out first that the overall reaction is predicted to be clearly exothermic and the dimeric product (**6**) represents the global minimum on the energy surface. The net energy of the formation of complex **6** (according to 2(**1**) + 2CO_2 → **6** + 4PMe_3) is −27 kcal/mol. All the key reaction intermediates (**2**−**5**) lie below the **1** + CO_2 level, and they are separated by reasonably low energy barriers. These results indicate that the series of elementary steps sketched in Figure 11 is a conceivable energy path from **1** + CO_2 to the dimeric hydrido-acrylate product providing theoretical support for the reaction mechanism proposed by Carmona et al.[22,23]

Our results are consistent with the picture that the reaction is initiated by the **1** + CO_2 → **2** + PMe_3 substitution step, which occurs easily via a dissociative mechanism (**1** → **1′** + PMe_3, **1′** + CO_2 → **2**) owing to the loose nature of the reactant tetraphosphine complex. The substitution is slightly exothermic, and it leads to complex **2**, which is a key intermediate in the CO_2−C_2H_4 coupling process. The oxidative C−C coupling is one of the most costly steps on the reaction path; its activation barrier is estimated to be 11 kcal/mol. However, the formation of the metalla-lactone species (**3**) from **2** is thermodynamically allowed.

Another important point to be noticed in the energy profile is that the metalla-lactone structure, which is found to be the final product in a number of CO_2−alkene coupling reactions,[14−21] does not represent a thermodynamic sink on the reaction path. This intermediate can rearrange to an agostic complex (**4**), which then undergoes β-hydrogen transfer to give the hydrido-acrylate monomer (**5**). One possible route for the **3** → **4** rearrangement involves phosphine exchange (**3** → **3″**) followed by the **3″** → **4** step, but other low energy **3** → **4** transformations stemming from the fluxional nature of related compounds are also conceivable, although we found no evidence for a simple internal rotation pathway. The hydride formation from **4** is an exothermic step; however, the related activation barrier (10 kcal/mol) is comparable to that of the C−C coupling. On the other hand, the activation energy of the reverse reaction, that is, the **5** → **4** migratory olefin insertion, is notably higher suggesting that the hydride formation is likely an irreversible step.

The hydrido-acrylate monomer is already well below the energy of the reactants, but further stabilization is achieved by

(66) For previous work on including solvation in modeling catalytic mechanisms, see for example: Das, P. K.; Dockter, D. W.; Hahey, D. R.; Lauffer, D. E.; Hawkins, G. D.; Li, J.; Zhu, T.; Cramer, C. J.; Truhlar, D. G.; Dapprich, S.; Froese, R. D. J.; Holthausen, M. C.; Liu, Z.; Mogi, K.; Vyboishchikov, S.; Musaev, D. G.; Morokuma, K. In *Transition State Modeling for Catalysis*; Truhlar, D. G., Morokuma, K., Eds.; ACS Symposium Series 721; American Chemical Society: Washington, DC, 1999; pp 208−224.

(67) We have estimated the solvation energies by using the conductor-like screening model (COSMO) as well (see ref 68) as that implemented in ADF (ref 69) and found only minor differences in the stabilization energies computed by the two models. Namely, the stabilization energies obtained from COSMO-BP86/STO calculations for the stationary points were systematically larger by 1−2 kcal/mol than those from the PCM model.

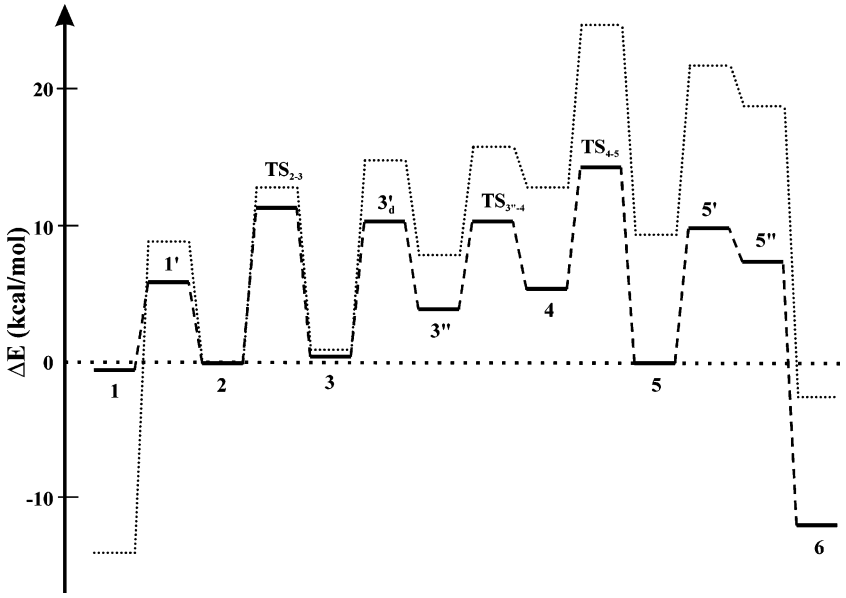

Figure 12. Energy profiles corresponding to the gas-phase $PR_3 = PMe_3$ (dashed) and $PR_3 = PH_3$ (dotted) models (see ΔE_g values in Table 1). The reference energy level is chosen at **2** + P for both models.

the dimerization process. The dimerization can take place relatively easily because the dissociation of a PMe_3 ligand is facilitated by the *trans*-effect of the metal-hydride bond in **5** and the formed acrylate group allows the bridge formation between two enantiomeric monomers. We note that mononuclear hydrido-acrylates have also been synthesized before by substituting two PMe_3 ligands in **1** by chelating phosphines such as $Et_2PCH_2CH_2PEt_2$ (depe), for instance, and reacting the *trans*-$[M(C_2H_4)_2(depe)(PMe_3)_2]$ complex with CO_2.[24] Assuming that this reaction follows a similar route that we considered here, the complex analogous to **5** necessarily involves a bidentate phosphine with one of its P atoms in trans position to the hydride bond. The chelating effect, however, prevents the phosphine dissociation, the dimerization is blocked, and the mononuclear species is to be considered as the final product.

Returning to the energy profile, it is quite impossible to give any firm conclusion about the rate determining step of the present reaction. This is not only because we found several steps with comparable activation barriers, but also because the reaction pathway is a combination of uni- and bimolecular steps and a complete kinetic analysis would be required to estimate the relevant rate constants.

4.8. Issue of Model Truncation. We have already pointed out that the replacement of the PMe_3 ligands by PH_3 groups implies severe inaccuracies in the structure and the stability of the initial $Mo(C_2H_4)_2(PMe_3)_4$ complex and this approximation gives a rather unreliable energy for the **1** → **1′** + PMe_3 dissociation step. This type of model simplification is quite often introduced in theoretical studies, mostly to reduce computational demands. Therefore, it is interesting to parallel the entire $PR_3 = PH_3$ and $PR_3 = PMe_3$ energy profiles. The smaller model also provides data to estimate the zero-point energy (ZPE) corrections and the entropic effects upon the energetics of the reaction since the harmonic vibrational frequencies are available for each stationary point on the $PR_3 = PH_3$ potential surface. In Table 1, we supplemented the $PR_3 = PMe_3$ data with the gas phase relative electronic energies, their ZPE corrected values, and the corresponding free energy variations related to the truncated model.

To highlight the discrepancies between the results of the two models, we plotted the gas phase energy profiles in Figure 12. Here, the reference energy level has been arbitrarily chosen at **2** + PR_3, so as to separate the error involved already in the first step in the $PR_3 = PH_3$ calculations from those regarding the remaining part of the reaction pathway. It is apparent from Figure 12 that the predicted relative energies are less sensitive to the choice of the model than that obtained for the PMe_3 dissociation energy. For instance, the binding energy of CO_2 in the simplified analogue of **2** is predicted to be 9.0 kcal/mol, which is only 3 kcal/mol larger than the value calculated with the more realistic model (see the **1′** + CO_2 → **2** step in Figure 12). This can clearly be attributed to the reduction of repulsive interactions between the coordinated ligands in the unsaturated triphosphine intermediate and in the CO_2 complex as well.

The comparison in Figure 12 also shows that the truncated model systematically overestimates the activation barriers by about 2−4 kcal/mol. This holds true not only for the barriers associated with the dissociation of the phosphines but also for those related to the CO_2−C_2H_4 coupling and the β-hydrogen transfer steps. These errors add up gradually along the pathway, and as a result, the intermediates and the final product become highly unstable on the $PR_3 = PH_3$ potential surface. Because the steric congestion is greatly reduced after the **1** → **1′** + PMe_3 dissociation step, the discrepancies can only be partially attributed to steric effects. For example, the differences seen for the activation energies of the oxidative coupling and the β-hydrogen transfer steps should be related to the electron-donating abilities of the phosphines. As PMe_3 is a better σ-donor, it facilitates the oxidation of the metal atom occurring in these processes and stabilizes the corresponding transition states.

The comparison of the ΔE_g and ΔE_g^{ZPE} values shown for $PR_3 = PH_3$ in Table 1 illustrates that the inclusion of ZPE corrections has only a slight influence on the relative stability of the stationary points. Most of the reaction intermediates have similar relative energies as on the uncorrected potential surface, but the barriers associated with the phosphine dissociation steps are decreased by about 2 kcal/mol. The ZPE contribution at the stationary points lowers the effective barrier for CO_2−C_2H_4

coupling by less than a kcal/mol, but the effective barrier for the β-hydrogen shift is reduced by 2.4 kcal/mol. One would expect similar changes in ZPE for the PMe_3 case as those for the PH_3 one, so these conclusions should also hold for $PR_3 = PMe_3$. Comparison of ΔE_g and ΔG_g values in Table 1 reveals that the free energy profile of the reaction at the stationary points is almost identical to the energy profile, except for the phosphine dissociation steps ($\mathbf{1} \rightarrow \mathbf{1'} + PR_3$, $\mathbf{3} \rightarrow \mathbf{3'_d} + PR_3$ and $\mathbf{5} \rightarrow \mathbf{5'} + PR_3$), where entropic effects reduce the free energy barriers significantly. A more complete accounting for entropic effects would require computing the free energy profile not just at stationary points but all along the reaction path to find the variational transition state,[70] which would allow a variational calculation of activation energies as well.[71] An accurate calculation of the hydrogen transfer step would also require considering quantum mechanical tunneling.[72]

5. Concluding Remarks

While considerable successes have been achieved in the past decades in developing catalytic methods for C−C coupling reactions between CO_2 and unsaturated hydrocarbons, the refined understanding of the mechanism of these reactions is still lacking. The present work provides the first detailed theoretical mechanistic study on a metal-assisted $CO_2-C_2H_4$ coupling reaction. The system we have investigated here was thoroughly examined experimentally, and we strongly relied upon the experimental evidence in identifying the elementary steps of the reaction. We have shown that the mechanism suggested as the most conceivable route corresponds to a low energy reaction pathway on model potential energy surfaces.

One of the key intermediates along this pathway is a complex involving coordinated CO_2 and C_2H_4 ligands. The coupling takes place in the coplanar arrangement of the reacting ligands via a five-center transition state, resulting in a nearly planar metallalactone species. The present reaction thus constitutes an example where the coordination of the CO_2 molecule to the metal center is a necessary step to achieve the CO_2−alkene coupling because the formation of the new C−C bond is promoted by a simultaneous metal → CO_2 and metal → C_2H_4 electron-donation mechanism.

We described the structure and the relative stability of subsequent reaction intermediates and transition states as well. The five-membered metallacycle is found to be able to distort and adopt a structure involving β-agostic interactions. The agostic complex is also a crucial intermediate along the reaction path because it facilitates the formation of the metal-hydride species in a β-hydrogen transfer process. Although the dimerization of the hydrido-acrylate complex provides extra stabilization to the investigated system, this step is not necessarily required to have an exothermic energy balance since the formation of the monomeric species is already favored thermodynamically.

The present study indicates that the ancillary phosphine ligands play an important role in various phases of the reaction. The CO_2 coordination is made possible by a phosphine dissociation from the tetraphosphine reactant, which has a steric origin. Some of the rearrangement processes and the dimerization of the hydrido-acrylate species are also associated with phosphine dissociation. In addition to steric factors, electronic effects of the σ-donating phosphine ligands are of great importance too since the oxidative $CO_2-C_2H_4$ coupling is facilitated by σ-donation, because the metal atom acts as a basic center in the coupling process.

A few aspects of model construction relevant to the title reaction have also been investigated in the present work. We found that the model truncation introduced by substituting the real ligand, PMe_3, by PH_3 causes significant errors in energy predictions, and we showed that the inclusion of solvent effects is mandatory to obtain reliable reaction energy profiles.

The examined Mo-assisted acrylate formation represents an example of stoichiometric CO_2−olefin coupling reactions. Elucidating the mechanism of catalytic systems still remains a challenging area for further theoretical studies. We continue our investigations along these lines.

Acknowledgment. This work has been supported by the Hungarian Research Foundation (OTKA, F037345). Computer facilities provided by the NIIF Supercomputer Center in Budapest and by the Center of Information Systems of the Budapest University of Technology and Economics are greatly acknowledged. We thank Agustín Galindo for valuable discussions and Stephen A. Miller for critical comments.

Supporting Information Available: Cartesian coordinates of all stationary points located on the $PR_3 = PH_3$ and $PR_3 = PMe_3$ potential energy surfaces. This material is available free of charge via the Internet at http://pubs.acs.org.

JA035791U

(68) Klamt, A.; Schuurmann, G. *J. Chem. Soc., Perkin Trans.* **1993**, *2*, 799.
(69) Pye, C.; Ziegler, T. *Theor. Chem. Acc.* **1999**, *101*, 396.
(70) Garrett, B. C.; Truhlar, D. G. *J. Am. Chem. Soc.* **1979**, *101*, 4534.
(71) Garrett, B. C.; Truhlar, D. G.; Bowman, J. M.; Wagner, A. F.; Robie, D.; Arepalli, S.; Presser, N.; Gordon, R. J. *J. Am. Chem. Soc.* **1986**, *108*, 3515.
(72) Espinosa-Garcia, J.; Corchado, J. C.; Truhlar, D. G. *J. Am. Chem. Soc.* **1997**, *119*, 9891.